

Uncovering the mechanism of anthocyanin accumulation in a purple-leaved variety of foxtail millet (*Setaria italica*) by transcriptome analysis

Yaofei Zhao ^{Equal first author, 1}, Yaqiong Li ^{Equal first author, 1}, Xiaoxi Zhen ¹, Jinli Zhang ¹, Qianxiang Zhang ¹, Zhaowen Liu ¹, Shupei Hou ¹, Yuanhuai Han ^{Corresp., 1}, Bin Zhang ^{Corresp., 1}

Corresponding Authors: Yuanhuai Han, Bin Zhang Email address: hanyuanhuai@sxau.edu.cn, Abingood@126.com

Anthocyanin is a natural pigment that has a functional role in plants to attract pollinating insects and is important in stress response. Foxtail millet (*Setaria italica*) is a kind of nutritional crop with high resistance to drought and sterility. However, the molecular mechanism regulating anthocyanin accumulation and the relationship between anthocyanin and the stress resistance of foxtail millet remains obscure. In this study, we screened hundreds of germplasm resources and obtained several varieties with purple plants in foxtail millet. By studying the purple-leaved B100 variety and the control variety, Yugu1 with green leaves, we found that B100 could accumulate a large amount of anthocyanin in the leaf epiderma, and B100 had stronger stress tolerance. Further transcriptome analysis revealed the differences in gene expression patterns between the two varieties. We identified nine genes encoding enzymes related to anthocyanin biosynthesis using quantitative PCR validation that showed significantly higher expression levels in B100 than Yugu1. The results of this study lay the foundation for the analysis of the molecular mechanism of anthocyanin accumulation in foxtail millet, and provided genetic resources for the molecular breeding of crops with high anthocyanin content.

Shanxi Key Laboratory of Minor Crop Germplasm Innovation and Molecular Breeding, College of Agriculture, Shanxi Agricultural University, Taigu, Shanxi 030801. China



1 Uncovering the mechanism of anthocyanin

2 accumulation in a purple-leaved variety of foxtail

3 millet (Setaria italica) by transcriptome analysis

4
5 Yaofei Zhao ^{1,*}, Yaqiong Li ^{1,*}, Xiaoxi Zhen ¹, Jinli Zhang ¹, Qianxiang Zhang ¹, Zhaowen Liu ¹,

- 6 Shupei Hou ¹, Yuanhuai Han ^{1, #}, Bin Zhang ^{1, #}
- 7 ¹ Shanxi Key Laboratory of Minor Crop Germplasm Innovation and Molecular Breeding,
- 8 College of Agriculture, Shanxi Agricultural University, Taigu, Shanxi, China.
- 9 * These authors contributed equally to this work.
- 11 Corresponding Author:
- 12 Bin Zhang
- 13 Taigu, Shanxi 030801, China
- 14 Email address: Abingood@126.com
- 16 Yuanhuai Han
- 17 Taigu, Shanxi 030801, China
- 18 Email address: hanyuanhuai@sxau.edu.cn

19 20 21

10

15

Abstract

- 22 Anthocyanin is a natural pigment that has a functional role in plants to attract pollinating insects
- and is important in stress response. Foxtail millet (Setaria italica) is a kind of nutritional crop
- 24 with high resistance to drought and sterility. However, the molecular mechanism regulating
- 25 anthocyanin accumulation and the relationship between anthocyanin and the stress resistance of
- 26 foxtail millet remains obscure. In this study, we screened hundreds of germplasm resources and
- 27 obtained several varieties with purple plants in foxtail millet. By studying the purple-leaved
- 28 B100 variety and the control variety, Yugu1 with green leaves, we found that B100 could
- 29 accumulate a large amount of anthocyanin in the leaf epiderma, and B100 had stronger stress
- 30 tolerance. Further transcriptome analysis revealed the differences in gene expression patterns
- 31 between the two varieties. We identified nine genes encoding enzymes related to anthocyanin
- 32 biosynthesis using quantitative PCR validation that showed significantly higher expression levels
- in B100 than Yugu1. The results of this study lay the foundation for the analysis of the molecular



35	molecular breeding of crops with high anthocyanin content.
36	
37	Introduction
38	Flowers, fruits and seeds generally display different colors in nature to attract animal pollinators
39	or seed dispersers (Grotewold, 2006). The coloration is determined by the deposition of
40	pigments, including betalains, carotenoids and anthocyanins. Anthocyanins, which have been
41	studied most, are responsible for the red, blue and purple colors of plant tissues. Additionally,
42	anthocyanins have been found to perform pivotal roles in a plant's response to environmental
43	stresses. Anthocyanin accumulation can be induced by biotic or abiotic stresses including
44	pathogen infection, drought, salt, cold, mechanical damage and high light intensity (Albert et al.,
45	2009; An et al., 2020; An et al., 2019; Kim et al., 2017; Li et al., 2017; Naing et al., 2018;
46	Nakabayashi et al., 2014; Qin et al., 2020; Shen et al., 2017; Wang et al., 2018; Yong et al.,
47	2019). Anthocyanins have been found to have health-promoting factors which defend against
48	disease, improve immunity, and prevent cardiovascular diseases. Therefore, anthocyanins are of
49	great interest for research and practical applications (He & Giusti, 2010; Lila et al., 2016).
50	
51	Anthocyanins are derived from a branch of the flavonoid metabolism pathway in plants. The
52	biosynthesis of anthocyanins is catalyzed by a series of enzymes, such as chalcone synthase
53	(CHS), chalcone isomerase (CHI), flavanone 3-hydroxylase (F3H), dihydroflavonol 4-reductase
54	(DFR), anthocyanidin synthase (ANS), and UDP-3-O-glucosyltransferases (UFGT/3GT).
55	Anthocyanins are water-soluble, synthesized in the cytoplasm, and then transported to the
56	vacuole for storage (Koes et al., 2005). Anthocyanins are found in the flowers, fruits, seeds,
57	leaves, and stems, and their distribution varies based on plant species, plant tissues,
58	developmental stages and environmental factors. In Arabidopsis thaliana, anthocyanins are
59	distributed in the subcutaneous tissue cells of the adaxial side and epidermal cells of the abaxial
60	side of rosette leaves (Kubo et al., 1999). In red-leaved ornamental kale (Brassica oleracea var.
61	acephala DC) leaves, anthocyanins are distributed in epidermal cells and mesophyll cells
62	adjacent to the epidermis; however, there was no pigment deposition in the internal mesophyll
63	cells. Anthocyanin accumulation varied in young leaves and mature leaves of Mikania micrantha
64	under low-temperatures. Young leaves showed high pigment deposition in the adaxial and

mechanism of anthocyanin accumulation in foxtail millet, and provided genetic resources for the



65	abaxial sides, whereas mature leaves only had high pigment deposition in the abaxial side.
66	Additionally, the total antioxidant capacity of young leaves was significantly higher than that of
67	mature leaves, while the photosynthetic rate of mature leaves was significantly higher than that
68	of young leaves. Thus, plants can modulate anthocyanin distribution to adapt to different
69	environments (Zhang et al., 2019a).
70	
71	Foxtail millet (Setaria italica) is an important C ₄ cereal and forage crop, with high
72	photosynthetic efficiency and good adaptability to the environment. These advantages, together
73	with the properties of self-pollination, a small genome and extensive genetic diversity make
74	foxtail millet a model plant for the C ₄ cereal crop with tremendous potential. To further promote
75	the development of functional genomics of foxtail millet, researchers identified a mutant
76	(xiaomi) with a similar life cycle and size to Arabidopsis (Yang et al., 2020). High quality
77	reference genomes were assembled, a multi-omics database was constructed, and a highly
78	efficient genetic transformation system was established to explore the genetic resources and
79	molecular breeding of cereal grains. Although the biological function and metabolic mechanism
80	of anthocyanins have been extensively studied in some plants such as Arabidopsis, maize (Zea
81	mays), tomato (Lycopersicon esculentum), and snapdragon (Antirrhinum majus), the research in
82	foxtail millet is still in its infancy (Albert et al., 2021; Petroni & Tonelli, 2011; Sun et al., 2020).
83	In this study, purple- and green-leaved foxtail millet varieties were used as experimental
84	materials to analyze the distribution of anthocyanin, physiological indexes, and transcriptome
85	sequencing analysis. The results of our study will help to explore the mechanism of anthocyanin
86	accumulation in foxtail millet and lay a foundation for the further study of the molecular
87	mechanism of anthocyanin synthesis regulation in foxtail millet.
88	
89	Materials & Methods
90	Plant material and growth conditions
91	The seeds of foxtail millet varieties B100 (purple-leaved variety) and Yugu 1 (green-leaved
92	variety) were sown in an experimental plot located at 37 $^{\circ}$ N, 112 $^{\circ}$ E. The leaves were collected
93	for analysis when plants reached a mature four-leaf stage.
94	
95	Mornhological observations



- 96 The leaves were sliced using two, side-by-side blades for morphoanatomical evaluation. The
- 97 slices were embedded in water and were then observed under a microscope.

99

Measurement of plant pigments

- Anthocyanin was extracted from leaves with 0.1% HCl-methanol at 4°C for 12 hours in dark.
- The absorption values of the extraction were measured at 530 and 700 nm wavelengths using the
- mixture of supernatant and reagent 1 (50 mmol·L⁻¹ KCl, 150 mmol·L⁻¹ HCl, pH=1.0), followed
- by the mixture of supernatant and reagent 2 (100 mmol·L⁻¹ NaAC, 240 mmol·L⁻¹ HCl, pH=4.5).
- 104 The method of calculation was as follows (Luo et al., 2017):
- 105 Anthocyanin (mg/g·FW) = $[(A_{520}-A_{700})_{\text{reagent 1}} (A_{520}-A_{700})_{\text{reagent 2}}] \times M \times V \times n / (\epsilon \times m)$
- 106 M: relative molecular weight of anthocyanins, 449.2 g/mol; V: extraction volume; ε: molar
- extinction coefficient of anthocyanins, 2.69 × 104 L/mol/cm; n: dilution times; m: sample
- 108 weight.
- 109 Chlorophyll and carotenoids were extracted from leaves using 80% acetone for 24 h. Then the
- absorption values were measured from the extraction at 663, 646 and 470 nm wavelengths
- 111 (Porra, 2002). The method of calculation was as follows (V: extraction volume, W: sample
- 112 weight):
- 113 Chlorophyll a $(mg/g \cdot Fw) = (12.21A_{663} 2.81A_{646}) \times V/W \times 1000$
- 114 Chlorophyll b (mg/g·Fw) = $(20.13A_{646} 5.03A_{663}) \times V/W \times 1000$
- 115 Chlorophyll (mg/g·Fw) = chlorophyll a (mg/g·Fw) + chlorophyll b (mg/g·Fw)
- 116 Carotenoid (mg/g·Fw) = $[1000A_{470} 3.27 \times (12.21A_{663} 2.81A_{646}) 104 \times (20.13A_{646} 10.000)]$
- 117 $5.03A_{663}$)] /229 × V/ W×1000
- 118 The raw data of the pigment measurement is shown in Supplemental Table 5.

119

120 Total antioxidant capacity assay

- 121 Antioxidants were extracted from leaves with 80% methanol. The antioxidant capacity was
- measured using the ferric-reducing antioxidant power (FRAP) method. [citation?]
- 123 Trolox solutions were prepared using methanol as the solvent of gradient concentrations. The
- 124 Trolox solutions and FRAP solution were mixed for reaction for 1 hour in the dark. Then we



125	measured the absorption value of the mixture at 593 nm wavelength. The standard curve was
126	drawn by taking the Trolox concentration as the x-axis and the absorbance as the y-axis.
127	The leaf extracts and FRAP solution were mixed for reaction for 1 hour in the dark. Then we
128	measured the absorption value of the mixture at 596 nm wavelength. The antioxidant capacity
129	was assayed according to the standard curve and absorbance. The raw data of this assay is shown
130	in Supplemental Table 6.
131	
132	Measurement of soluble sugar content
133	The leaves were homogenized with 80% ethanol and were extracted at 80°C for 30 min. The
134	supernatant was transferred to a fresh, clean tube after centrifugation at 3,500 g for 10 min. The
135	sediment was then extracted twice using the above procedure with 80% ethanol. The supernatant
136	was added into an anthrone-sulfuric acid reagent and was boiled for 10 min. After cooling to
137	room temperature, the absorption value of the extraction was measured at 620 nm (Leng et al.,
138	2016). The raw data of this assay is shown in Supplemental Table 6.
139	
140	Transcriptome sequencing and analyses
141	The total RNA was extracted from leaves using RNAiso Plus (9109; Takara). The RNA
142	preparations were evaluated with agarose gel electrophoresis and were quantified using a
143	microultraviolet-visible fluorescence spectrophotometer.
144	Three biological replicates of both Yugu1 and B100 were used in RNA-sequencing. The
145	statistical power of this study was calculated using RNASeqPower
146	(https://bioconductor.org/packages/release/bioc/html/RNASeqPower.html) as $P < 0.05$. The
147	quality control of raw data was performed as previous study (Wang et al., 2017). We retrieved
148	144,677,546 clean reads, including 43.4 G total bases. The sequencing depth was 100x. The
149	clean data were aligned to the foxtail millet genome (Yugu1) using HISAT2 software (Kim et al.
150	2015), and the mapped reads were analyzed by String Tie software (Pertea et al. 2015). The
151	abundance of transcripts was normalized using the fragments per kilobase of transcript per
152	million mapped reads (FPKM) method. Prior to differential gene expression analysis, for each
153	sequenced library, the read counts were adjusted using the edgeR program package with one
154	scaling normalized factor. Differential expression analysis of the two samples was performed
155	using the EBSeq R package. The resulting false discovery rate (FDR) was adjusted using the

et al., 2010).



156	posterior probability of being DE (PPDE). The FDR $< 0.05 \& log2 $ (foldchange) $ \ge 1$ was set
157	as the threshold for significantly differential expression. Differential expression analysis of the
158	two conditions/groups was performed using the DESeq R package (1.10.1). DESeq provided
159	statistical routines for determining the differential expression in digital gene expression data
160	using a model based on the negative binomial distribution. The resulting P values were adjusted
161	using the Benjamini and Hochberg's approach for controlling the FDR. Genes with an adjusted
162	P-value < 0.05 by DESeq were assigned as differentially expressed. R package method (Young
163	We performed Gene Ontology (GO) enrichment analysis by the GOseq R packages which is a
164	known method (Young et al., 2010). The KEGG database (http://www.genome.jp/kegg/) was
165	used to discover the regulatory pathways of genes (Kanehisa et al., 2008). We used KOBAS
166	(Mao et al., 2005) to determine the enrichment of DEGs in KEGG pathways.
167	The raw data of the RNA sequencing was submitted to an SRA database (BioProject accession
168	number: PRJNA777600).
169	
170	Quantitative real-time PCR analysis
171	The total RNA was isolated as mentioned above. The first-strand cDNA was synthesized using
172	the PrimeScript RT reagent kit with gDNA Eraser (RR047A; Takara). qRT-PCR was performed
173	using the Bio-Rad CFX96TM Touch real-time PCR detection system with SYBR Premix Ex
174	TaqTM II (Tli RNaseH Plus) (RR820A; Takara). Transcript levels were normalized to the
175	SiActin (Seita.5G464000). The raw data of qRT-PCR is shown in Supplemental Table 7. The 2^-
176	$\Delta\Delta Ct$ method was used to calculate the expression level of the genes and the one-way ANOVA
177	was used to identify significant differences (http://vassarstats.net/anovalu.html).
178	
179	Results
180	Purple-leaved variety B100 accumulated more anthocyanin than YG1 in epidermal cells
181	In a previous study, we obtained a few foxtail millet varieties with different leaf colors, stems
182	and panicles. We selected two representative varieties B100 (purple-leaved variety) and Yugu1
183	(YG1, green-leaved variety) to analyze the variation of anthocyanin distribution in foxtail millet.
184	The morphology characteristics showed that B100 presented the visible purple color of the
185	leaves at the seedling stage but the leaves of YG1 were green (Figure 1A). Furthermore, the
186	leaves of B100 and YG1 showed a different color at the maturation stages (Figure 1B). The



187	purple color of the purple leaves was deepest in the vein, which implied that anthocyanin was
188	transported through the vascular bundle. Anatomical observations of the leaf revealed that in the
189	leaves of B100, purple pigmentation was present in the adaxial and abaxial epidermal cells as
190	well as adjacent mesophyll cells, whereas the purple pigmentation was not significantly present
191	in the leaves of YG1 (Figures 1C-1D).
192	
193	The content of anthocyanin, not other pigments, was higher in B100 than YG1
194	We quantitatively analyzed the content of some pigments in B100 and YG1 to examine whether
195	the visible purple was due to an increase in anthocyanin accumulation. The results showed that
196	the anthocyanin content in B100 was significantly higher than YG1 at the seedling stage and the
197	maturation stage (Figure 2A), while the chlorophyll and carotenoid contents were higher in YG1
198	than in B100 (Figures 2B-2C). Furthermore, all three pigments contents were higher at the
199	maturation stage than at the seedling stage and the anthocyanin content was similar at the two
200	stages in YG1.
201	
202	B100 displayed enhanced stress resistance
203	Since anthocyanin synthesis and accumulation are closely related to the stress responses in
204	plants, we explored the functions of anthocyanin in regulating stress resistance in foxtail millet.
205	The total antioxidant capacity analysis was performed using the ferric-reducing antioxidant
206	power (FRAP) method and we established the standard curve (Supplemental Figure 1A). B100
207	was shown to accumulate more anthocyanin and was better able to scavenge free radical and
208	reductive ferrous ions than YG1 (Figure 3A). Meanwhile, B100 could accumulate more soluble
209	sugar in both the seedling and maturation stages compared to YG1 (Figure 3B). The standard
210	curve of the quantitative determination of soluble sugar is shown in Supplemental Figure 1B.
211	
212	Differentially expressed genes were identified through the analysis of transcriptome
213	characteristics in purple- and green-leaved foxtail millet varieties
214	We conducted RNA sequencing to elucidate the molecular mechanism underlying the
215	phenotypic and functional differences between the purple- and green-leaved varieties. The total
216	RNA of B100 and YG1 was extracted from the top second leaf at the maturation stage. The
217	quality of the RNA was detected by agarose gel electrophoresis (Supplemental Figure 2A), and

PeerJ

218	all RNA of corresponding samples that fulfilled the requirements were used for RNA-
219	sequencing. A total of 144,677,546 clean reads were obtained, with a total base number of 43.4
220	G and GC contents were between 58.24% and 59.01%. The quality values of the sequencing data
221	were statistically assessed for each sample of three biological replicates. The Q30 values were all
222	above 92.84%, indicating that the transcriptome data were of high quality and could be further
223	analyzed (Supplemental Table 1).
224 225	[assembly version? availability?] The clean reads were sequentially compared with the reference genome, YG1. Approximately
226	90.38%-91.50% of the clean reads in YG1 were sequentially compared to the reference genome.
227	In the purple-leaved variety B100, 88.05%-89.97% of reads were compared to the reference
228	genome. Among them, the proportion of clean reads with multiple locations was between 1.42%
229	and 1.72%, and the number of reads compared to the positive and negative strands of the genome
230	was similar. Therefore, the selected reference millet genome assembly may meet the needs for
231	analysis (Supplemental Table 2). We then obtained 1,184 significant differentially expressed
232	genes (DEGs) of YG1 and B100, in which 598 genes were up-regulated and 588 genes were
233	down-regulated in B100 compared with YG1 (Supplemental Figure 2B). A cluster analysis of
234	these genes was conducted by hierarchical clustering. According to the different expression
235	patterns, these DEGs were clustered into three groups. The genes in cluster I were down-
236	regulated in B100, and the genes in cluster III were up-regulated in B100 (Figure 4).
237	
238	Subsequently, enrichment analysis of DEGs was performed based on Gene Ontology (GO)
239	analysis and Kyoto Encyclopedia of Genes and Genomes (KEGG) pathway analysis. GO
240	analysis showed that DEGs were significantly enriched in the metabolic process, cell and cell
241	part, binding, and catalytic activity (Figure 5). KEGG pathway analysis revealed that the DEGs
242	were mainly enriched in the metabolic pathways. Among these DEGs, we identified some genes
243	encoding synthetase of flavonoid biosynthesis and phenylpropane biosynthesis which may be
244	related to anthocyanin metabolism (Figure 6).
245	
246	Nine structural genes related to anthocyanin biosynthesis may function in the accumulation
247	of anthocyanin





We screened nine structural genes involved in anthocyanin biosynthesis from the results of the
significant differentially expressed genes analysis that were up-regulated in B100 compared to
YG1. We performed quantitative real-time PCR to verify the results of RNA sequencing in
foxtail millet to determine the major role of these genes. As shown in Figure 7, the relative
expression levels of all nine structural genes in B100 were significantly higher than YG1 at the
maturation stage. Among these up-regulated genes, DFR (Seita.5G237900), LDOX-2
(Seita.1G000700) and AT (Seita.9G002300) had higher expression levels in B100 than YG1 at
both the seedling and maturation stages. With the development of foxtail millet, most of these
structural genes displayed an increasing expression level. However, the plant accumulated more
transcripts of PAL (Seita.1G240200) and UFGT (Seita.3G190000) at the seedling stage. All of
the nine DEGs in the B100 purple-leaved variety were up-regulated, which was consistent with
the results of RNA-sequencing. Moreover, the correlation between qRT-PCR and RNA-
sequencing was 0.9625 (Supplemental Figure 3). These results showed that the sequencing
results had high accuracy and reliability, and may be used for further investigations.
Discussion
Compared with other crops, foxtail millet has many elite traits, including high tolerance to
abiotic stresses and low requirement of fertilizer in cultivation, which make foxtail millet an
ideal staple food crop widely cultivated in semi-arid regions or infertile land (Muthamilarasan &
Prasad, 2021). Foxtail millet is also an important crop to ensure food and nutritional security in
the face of a rapidly expanding world population (Peng & Zhang, 2020). The purple-leaved B100
displayed an enhanced resistance to stresses, which may be due to anthocyanin accumulation.
Anthocyanins can improve the antioxidant capacity of plants. Under various stresses, plants
produce reactive oxygen species (ROS) which damage cells. In order to survive under stress,
ROS and damage to cells, excessive ROS must be scavenged in a timely manner and
anthocyanins play an important role in this process (Naing & Kim, 2021).
Recent research has focused on constituents (e.g., proteins and secondary metabolites) with
beneficial effects on human health (Sachdev et al., 2021). As natural pigments, anthocyanins are
not only accumulated in flowers, fruits and seeds to give them brilliant colors, but they are also
deposited in the vegetative organs such as leaves and stems. These pigments have protective and





280

281

282

283

284

285

286

287

288

289

290

291

292

293

294

295

296

297

298

299

300

301

302

303

304

305

306

307

308

309

defensive roles. Our study showed that the anthocyanin accumulation in the purple-leaved variety of foxtail millet was significantly higher than that in green-leaved variety, and that the antioxidant capacity was also higher in the purple-leaved variety. These results suggested that the purple-leaved variety may improve stress resistance through the accumulation of more anthocyanins. In future studies, we will analyze the differences in resistance to adversity between purple- and green-leaved varieties to explore the relationship between anthocyanin accumulation and stress responses in foxtail millet. Through previous studies of germplasm resources, we identified approximately 100 purple-leaved varieties of foxtail millet. Some of these showed enhanced resistance to abiotic stress. There may be a potential relationship between the secondary metabolites and their responses to abiotic stress. Our work is expected to reveal the regulatory mechanism of anthocyanin synthesis and the molecular basis of the high stress resistance of foxtail millet. The distribution of anthocyanins in plants is not uniform, and variations are seen with plant species, growth stage and environments (Guo et al., 2019; Zhang et al., 2019a). Through observing leaves throughout the entire growth period, we found that leaves of the purple-leaved variety were only purple during the seedling and maturation stages but were green in other growth stages. This phenomenon may be due to the fact that plants need to enhance photosynthesis to provide the energy needed for growth at the jointing and heading stages. Anthocyanin biosynthesis in plants is the results of a series of enzymatic reactions involving many enzymes. The first stage is phenylpropanoid biosynthesis from phenylalanine to pcoumaroyl-CoA. PAL and 4CL are the key enzymes of this stage. p-coumaroyl-CoA is then catalyzed to anthocyanins through flavonoid biosynthesis catalyzed by DFR and other key enzymes (LaFountain & Yuan, 2021). Genes encoding these enzymes are collectively referred to as structural genes (Holton & Cornish, 1995). Through transcriptome analysis, we discovered that the expression levels of nine structural genes in the purple-leaved variety were higher than that in green-leaved variety. These results indicate that these genes were closely related to the accumulation of anthocyanin in foxtail millet. It has been demonstrated that anthocyanin biosynthesis was affected by structural genes and regulatory genes. The proteins encoded by regulatory genes affect the accumulation of anthocyanin by regulating the expression of the



310	structural genes. The R2R3 MYB transcription factors, the basic-helix-loop-helix (bHLH)
311	transcription factors, and the WD40-repeat proteins can control the expression of anthocyanin
312	biosynthesis genes by forming a regulatory complex (Xu & Zhang, 2015). Researchers found
313	that the purple color of the pulvinus and leaf sheath of the foxtail millet paternal variety Shi-Li-
314	Xiang (SLX) is caused by the interaction between the bHLH transcription factor PPLS1 and
315	MYB transcription factor SiMYB85 promoting anthocyanin accumulation (Bai et al., 2020). Our
316	transcriptome data also showed that the expression levels of some regulatory genes varied in
317	purple- and green-leaved foxtail millet varieties. In future studies, we will explore the functions
318	of these regulatory genes in anthocyanin accumulation in foxtail millet. B100 and Yugu1 have
319	diverse genetic backgrounds and we will perform the whole-genome re-sequencing of B100 to
320	discover more genetic variations associated with anthocyanin accumulation. There are some
321	DEGs that have no relation with anthocyanin. However, some changes of gene expression
322	between B100 and Yugu1 may be the result of anthocyanin up-regulation, such as DEGs that are
323	mainly enriched in the plant-pathogen interaction. Anthocyanin accumulation has also been
324	reported to be related to plant immunity (Zhang et al., 2019b).
325	
326	China is one of the largest growers of foxtail millet, and its diversified natural and geographical
327	conditions have produced rich germplasm resources. B100 is not a widely grown variety due to
328	its low yield, however, it may have other functional uses. There are many arid and barren lands
329	in developing areas that are not suitable for general crops. Varieties with high stress resistance
330	like B100 are promising for their use in land utilization in severely arid regions. We have
331	identified a great number of foxtail millet varieties which contains large amounts of anthocyanin
332	and purple tissues. The stems and leaves of millet with high anthocyanin content can be used as
333	high-quality forage grass to enhance the economic value of animal products. However, we have
334	not found any variety that accumulated abundant anthocyanin in the endosperm. We will further
335	explore the differentially expressed genes, analyze the tissue specificity of their expression, and
336	promote the breeding of varieties of foxtail millet with high anthocyanin grains to meet the
337	health needs of humans.

Conclusions

338

339



- Foxtail millet is characterized by strong stress resistance and a rich nutritional content, however,
- 341 the mechanisms of metabolites synthesis and stress resistance regulation are not clear. The
- 342 identification and annotation of DEGs through RNA-sequencing suggested nine structural genes
- 343 that played important roles in regulating the accumulation of anthocyanin. As the secondary
- metabolite, anthocyanin plays an important role in regulating a plant's response to stress. The
- research on the regulatory network of anthocyanin synthesis will provide a theoretical basis for
- 346 high quality and highly stress-resistant crop breeding.

Author contribution statement

- 349 Z.B., H.Y., Z.Y. and L.Y. designed the experiments. Z.Y and L.Y performed most of the
- experiments. Z.X., Z.J., Z.Q., L.Z and H.S. assisted in materials preparation and data analysis.
- 351 Z.Y, L.Y., H.Y. and Z.B. wrote the article. All authors read and approved the final manuscript.

352

353 Funding

- 354 This work was funded by the National Natural Science Foundation of China (General Program,
- 355 32070366 and 31971906), Shanxi Province Science Found for Excellent Young Scholar
- 356 (201901D211382), and Scientific and Technological Innovation Programs of Higher Education
- 357 Institutions in Shanxi/ STIP (2020L0131 and 2021L118).

358 359

360

361

362

363

364

365

366

367

368

369

370

371

372

373

374

375

376

377

378

379

References

- Albert NW, Butelli E, Moss SMA, Piazza P, Waite CN, Schwinn KE, Davies KM, and Martin C. 2021. Discrete bHLH transcription factors play functionally overlapping roles in pigmentation patterning in flowers of Antirrhinum majus. *New Phytol* 231:849-863. 10.1111/nph.17142
- Albert NW, Lewis DH, Zhang H, Irving LJ, Jameson PE, and Davies KM. 2009. Light-induced vegetative anthocyanin pigmentation in Petunia. *J Exp Bot* 60:2191-2202. 10.1093/jxb/erp097
- An JP, Zhang XW, Bi SQ, You CX, Wang XF, and Hao YJ. 2020. The ERF transcription factor MdERF38 promotes drought stress-induced anthocyanin biosynthesis in apple. *Plant J* 101:573-589. 10.1111/tpj.14555
- An JP, Zhang XW, You CX, Bi SQ, Wang XF, and Hao YJ. 2019. MdWRKY40 promotes wounding-induced anthocyanin biosynthesis in association with MdMYB1 and undergoes MdBT2-mediated degradation. *New Phytol* 224:380-395. 10.1111/nph.16008
- Bai H, Song Z, Zhang Y, Li Z, Wang Y, Liu X, Ma J, Quan J, Wu X, Liu M, Zhou J, Dong Z, and Li D. 2020. The bHLH transcription factor PPLS1 regulates the color of pulvinus and leaf sheath in foxtail millet (Setaria italica). *Theor Appl Genet* 133:1911-1926. 10.1007/s00122-020-03566-4
- Grotewold E. 2006. The genetics and biochemistry of floral pigments. *Annu Rev Plant Biol* 57:761-780. 10.1146/annurev.arplant.57.032905.105248
- Guo N, Han S, Zong M, Wang G, Zheng S, and Liu F. 2019. Identification and differential expression analysis of anthocyanin biosynthetic genes in leaf color variants of ornamental kale. *BMC genomics* 20:564. 10.1186/s12864-019-5910-z
- He J, and Giusti MM. 2010. Anthocyanins: natural colorants with health-promoting properties. *Annu Rev Food Sci Technol* 1:163-187. 10.1146/annurev.food.080708.100754



- Holton TA, and Cornish EC. 1995. Genetics and Biochemistry of Anthocyanin Biosynthesis. *Plant Cell* 7:1071-1083. 10.1105/tpc.7.7.1071
- Kanehisa M, Araki M, Goto S, Hattori M, Hirakawa M, Itoh M, Katayama T, Kawashima S, Okuda S, Tokimatsu T,
 and Yamanishi Y. 2008. KEGG for linking genomes to life and the environment. *Nucleic Acids Res* 36:D480-484. 10.1093/nar/gkm882
 - Kim D, Langmead B, and Salzberg SL. 2015. HISAT: a fast spliced aligner with low memory requirements. *Nat Methods* 12:357-360. 10.1038/nmeth.3317
 - Kim J, Lee WJ, Vu TT, Jeong CY, Hong SW, and Lee H. 2017. High accumulation of anthocyanins via the ectopic expression of AtDFR confers significant salt stress tolerance in Brassica napus L. *Plant Cell Rep* 36:1215-1224. 10.1007/s00299-017-2147-7
 - Koes R, Verweij W, and Quattrocchio F. 2005. Flavonoids: a colorful model for the regulation and evolution of biochemical pathways. *Trends Plant Sci* 10:236-242. 10.1016/j.tplants.2005.03.002
 - Kubo H, Peeters AJ, Aarts MG, Pereira A, and Koornneef M. 1999. ANTHOCYANINLESS2, a homeobox gene affecting anthocyanin distribution and root development in Arabidopsis. *Plant Cell* 11:1217-1226. 10.1105/tpc.11.7.1217
 - LaFountain AM, and Yuan YW. 2021. Repressors of anthocyanin biosynthesis. *New Phytol* 231:933-949. 10.1111/nph.17397
 - Leng F, Sun S, Jing Y, Wang F, Wei Q, Wang X, and Zhu X. 2016. A rapid and sensitive method for determination of trace amounts of glucose by anthrone-sulfuric acid method. *Bulgarian Chemical Communications* 48:109-113.
 - Li P, Li YJ, Zhang FJ, Zhang GZ, Jiang XY, Yu HM, and Hou BK. 2017. The Arabidopsis UDP-glycosyltransferases UGT79B2 and UGT79B3, contribute to cold, salt and drought stress tolerance via modulating anthocyanin accumulation. *Plant J* 89:85-103. 10.1111/tpj.13324
 - Lila MA, Burton-Freeman B, Grace M, and Kalt W. 2016. Unraveling Anthocyanin Bioavailability for Human Health. *Annu Rev Food Sci Technol* 7:375-393. 10.1146/annurev-food-041715-033346
 - Luo J, Shi Q, Niu L, and Zhang Y. 2017. Transcriptomic Analysis of Leaf in Tree Peony Reveals Differentially Expressed Pigments Genes. *Molecules* 22. 10.3390/molecules22020324
 - Mao X, Cai T, Olyarchuk JG, and Wei L. 2005. Automated genome annotation and pathway identification using the KEGG Orthology (KO) as a controlled vocabulary. *Bioinformatics* 21:3787-3793. 10.1093/bioinformatics/bti430
 - Muthamilarasan M, and Prasad M. 2021. Small Millets for Enduring Food Security Amidst Pandemics. *Trends Plant Sci* 26:33-40. 10.1016/j.tplants.2020.08.008
 - Naing AH, Ai TN, Lim KB, Lee IJ, and Kim CK. 2018. Overexpression of Rosea1 From Snapdragon Enhances Anthocyanin Accumulation and Abiotic Stress Tolerance in Transgenic Tobacco. *Front Plant Sci* 9:1070. 10.3389/fpls.2018.01070
 - Naing AH, and Kim CK. 2021. Abiotic stress-induced anthocyanins in plants: Their role in tolerance to abiotic stresses. *Physiol Plant* 172:1711-1723. 10.1111/ppl.13373
 - Nakabayashi R, Yonekura-Sakakibara K, Urano K, Suzuki M, Yamada Y, Nishizawa T, Matsuda F, Kojima M, Sakakibara H, Shinozaki K, Michael AJ, Tohge T, Yamazaki M, and Saito K. 2014. Enhancement of oxidative and drought tolerance in Arabidopsis by overaccumulation of antioxidant flavonoids. *Plant J* 77:367-379. 10.1111/tpj.12388
 - Peng R, and Zhang B. 2020. Foxtail Millet: A New Model for C4 Plants. *Trends Plant Sci* 20:S1360-1385. 10.1016/j.tplants.2020.12.003
 - Pertea M, Pertea GM, Antonescu CM, Chang TC, Mendell JT, and Salzberg SL. 2015. StringTie enables improved reconstruction of a transcriptome from RNA-seq reads. *Nat Biotechnol* 33:290-295. 10.1038/nbt.3122
 - Petroni K, and Tonelli C. 2011. Recent advances on the regulation of anthocyanin synthesis in reproductive organs. *Plant science : an international journal of experimental plant biology* 181:219-229. 10.1016/j.plantsci.2011.05.009
 - Porra RJ. 2002. The chequered history of the development and use of simultaneous equations for the accurate determination of chlorophylls a and b. *Photosynth Res* 73:149-156. 10.1023/a:1020470224740
 - Qin L, Sun L, Wei L, Yuan J, Kong F, Zhang Y, Miao X, Xia G, and Liu S. 2020. Maize SRO1e represses anthocyanin synthesis through regulating the MBW complex in response to abiotic stress. *Plant J.* 10.1111/tpj.15083
- Sachdev N, Goomer S, and Singh LR. 2021. Foxtail millet: a potential crop to meet future demand scenario for alternative sustainable protein. *Journal of the Science of Food and Agriculture* 101:831-842. https://doi.org/10.1002/jsfa.10716
- Shen X, Guo X, Guo X, Zhao D, Zhao W, Chen J, and Li T. 2017. PacMYBA, a sweet cherry R2R3-MYB transcription





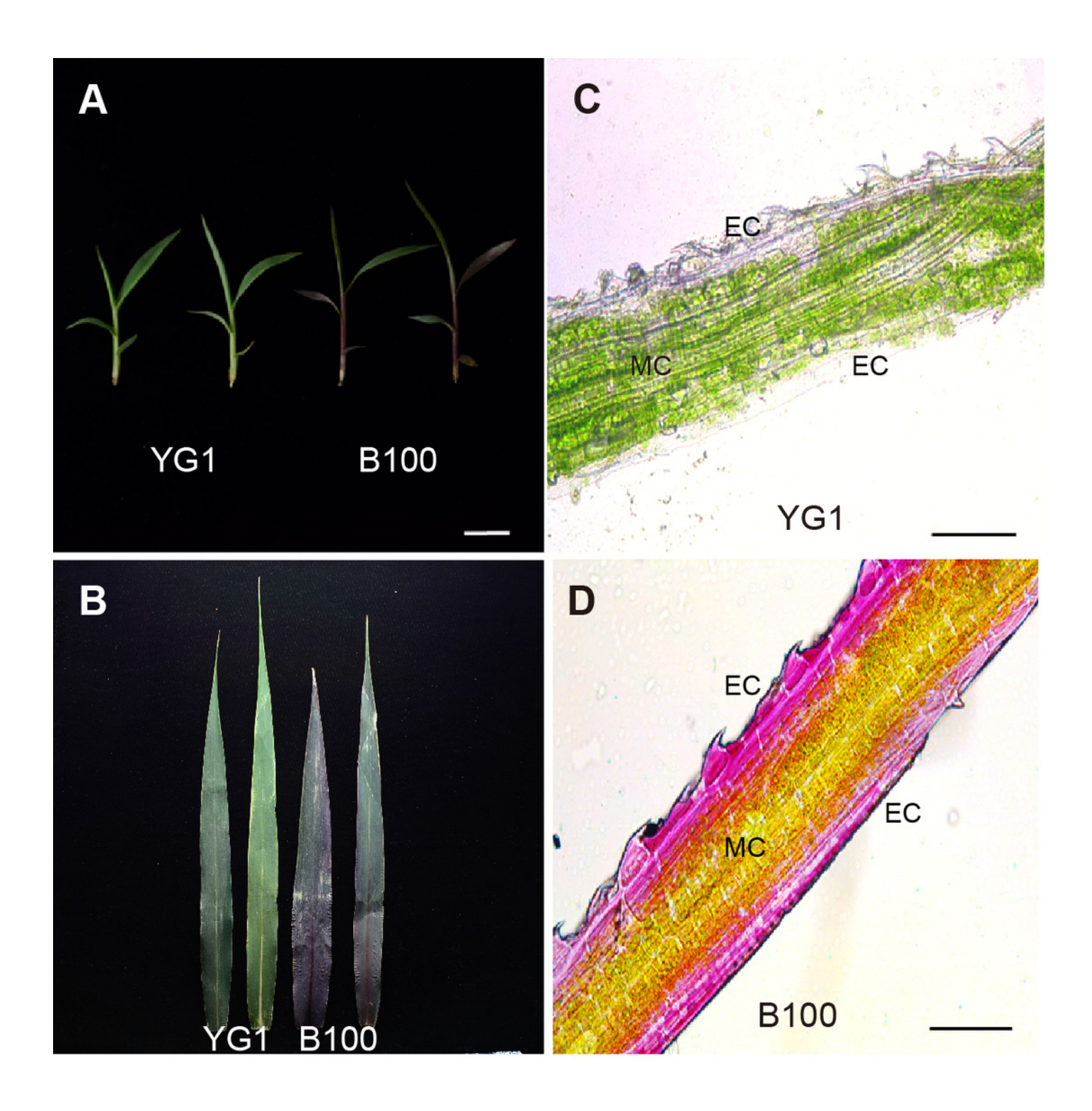
436	factor, is a positive regulator of salt stress tolerance and pathogen resistance. Plant Physiol Biochem 112:302-
437	311. 10.1016/j.plaphy.2017.01.015
438	Sun C. Deng L. Du M. Zhao J. Chen O. Huang T. Jiang H. Li CB. and Li C. 2020. A Transcriptional Network Promotes

- Sun C, Deng L, Du M, Zhao J, Chen Q, Huang T, Jiang H, Li CB, and Li C. 2020. A Transcriptional Network Promotes Anthocyanin Biosynthesis in Tomato Flesh. *Mol Plant* 13:42-58. 10.1016/j.molp.2019.10.010
- Wang N, Qu C, Jiang S, Chen Z, Xu H, Fang H, Su M, Zhang J, Wang Y, Liu W, Zhang Z, Lu N, and Chen X. 2018. The proanthocyanidin-specific transcription factor MdMYBPA1 initiates anthocyanin synthesis under low-temperature conditions in red-fleshed apples. *Plant J* 96:39-55. 10.1111/tpj.14013
- Wang Y, Wang Q, Gao L, Zhu B, Ju Z, Luo Y, and Zuo J. 2017. Parsing the Regulatory Network between Small RNAs and Target Genes in Ethylene Pathway in Tomato. *Front Plant Sci* 8:527. 10.3389/fpls.2017.00527
- Xu J, and Zhang S. 2015. Mitogen-activated protein kinase cascades in signaling plant growth and development. *Trends Plant Sci* 20:56-64. 10.1016/j.tplants.2014.10.001
- Yang Z, Zhang H, Li X, Shen H, Gao J, Hou S, Zhang B, Mayes S, Bennett M, Ma J, Wu C, Sui Y, Han Y, and Wang X. 2020. A mini foxtail millet with an Arabidopsis-like life cycle as a C4 model system. *Nature plants* 6:1167-1178. 10.1038/s41477-020-0747-7
- Yong Y, Zhang Y, and Lyu Y. 2019. A MYB-Related Transcription Factor from Lilium lancifolium L. (LlMYB3) Is Involved in Anthocyanin Biosynthesis Pathway and Enhances Multiple Abiotic Stress Tolerance in Arabidopsis thaliana. *Int J Mol Sci* 20. 10.3390/ijms20133195
- Young MD, Wakefield MJ, Smyth GK, and Oshlack A. 2010. Gene ontology analysis for RNA-seq: accounting for selection bias. *Genome Biol* 11:R14. 10.1186/gb-2010-11-2-r14
- Zhang Q, Zhai J, Chen G, Lin W, and Peng C. 2019a. The Changing Distribution of Anthocyanin in Mikania micrantha Leaves as an Adaption to Low-Temperature Environments. *Plants (Basel)* 8. 10.3390/plants8110456
- Zhang RX, Ge S, He J, Li S, Hao Y, Du H, Liu Z, Cheng R, Feng YQ, Xiong L, Li C, Hetherington AM, and Liang YK. 2019b. BIG regulates stomatal immunity and jasmonate production in Arabidopsis. *New Phytol* 222:335-348. 10.1111/nph.15568



Leaf phenotype analysis of YG1 and B100.

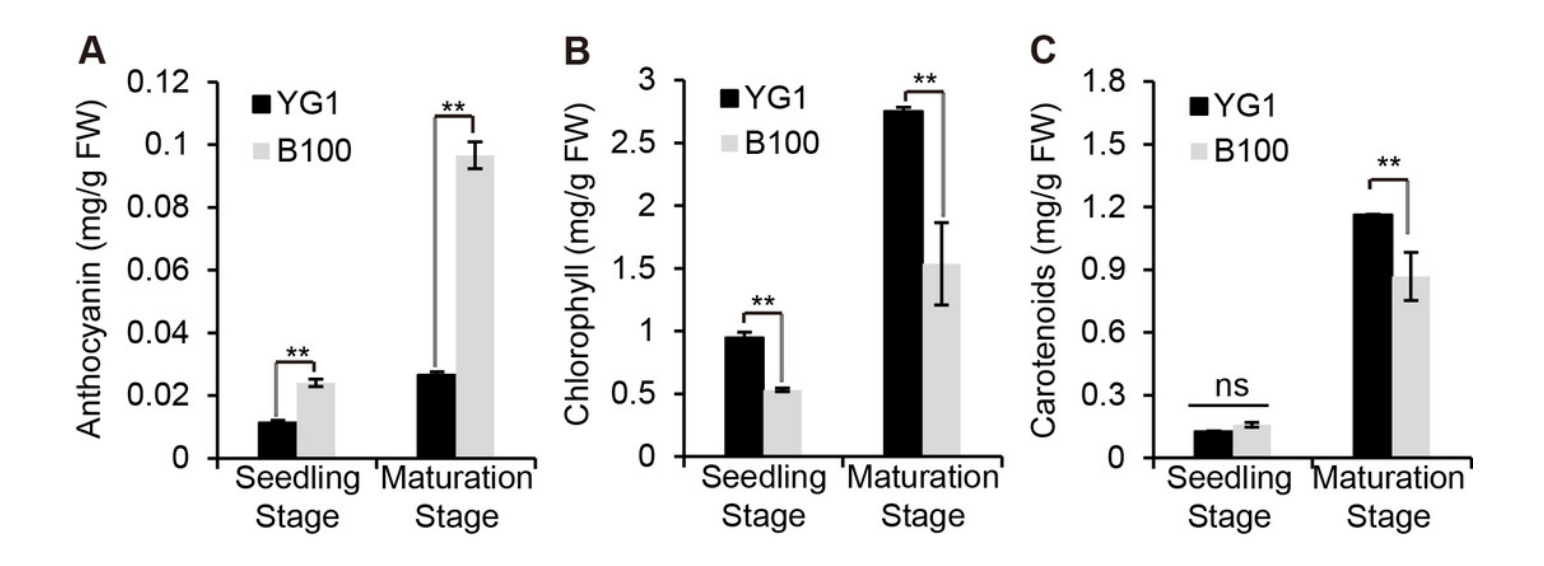
(A) Seedlings of YG1 and B100. Bar = 3 cm. (B) Flag leaves of YG1 and B100 in the maturing stage. Bar = 10 cm. (C-D) Transverse sections of YG1 leaves and B100 leaves, bars = 100 μ m. MC: mesophyll cells, EC: epidermal cells.





Quantitative analysis of plant pigments.

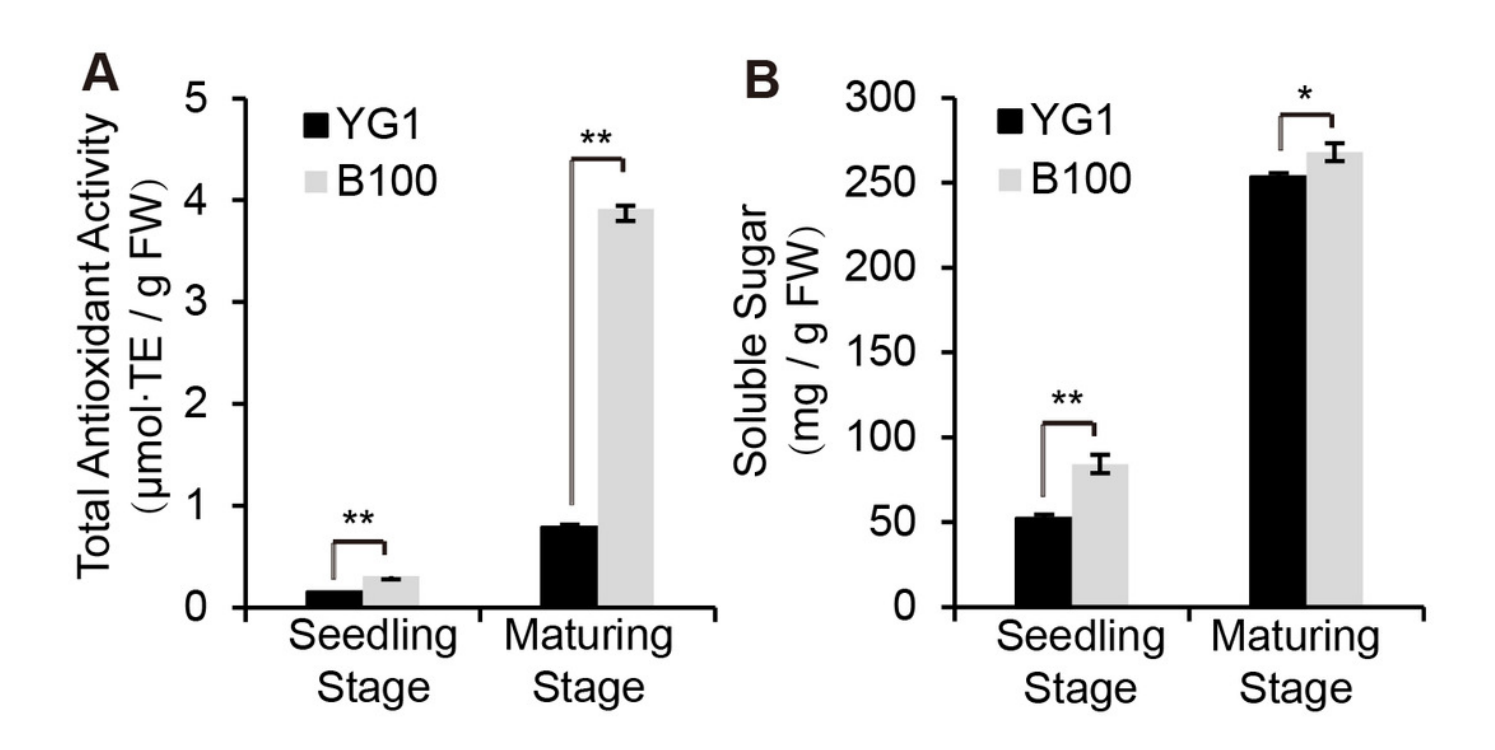
(A-C) The total content of anthocyanin, chlorophyll and carotenoids in leaves of YG1 and B100. Contents were detected at both the seedling and maturing stages. Bars represent means \pm SD of three biological replicates. Two asterisks (**) represent P < 0.01, ns represents no significant difference (n = 3, ANOVA). FW: fresh weight.





Quantitative analysis of physiological indexes to stress resistance.

The total antioxidant activity was determined using the FRAP method (A) and the total content of soluble sugar is shown. The bars represent the means \pm SD of three biological replicates. Two asterisks (**) represent P < 0.01 (n = 3, ANOVA). FW: fresh weight.

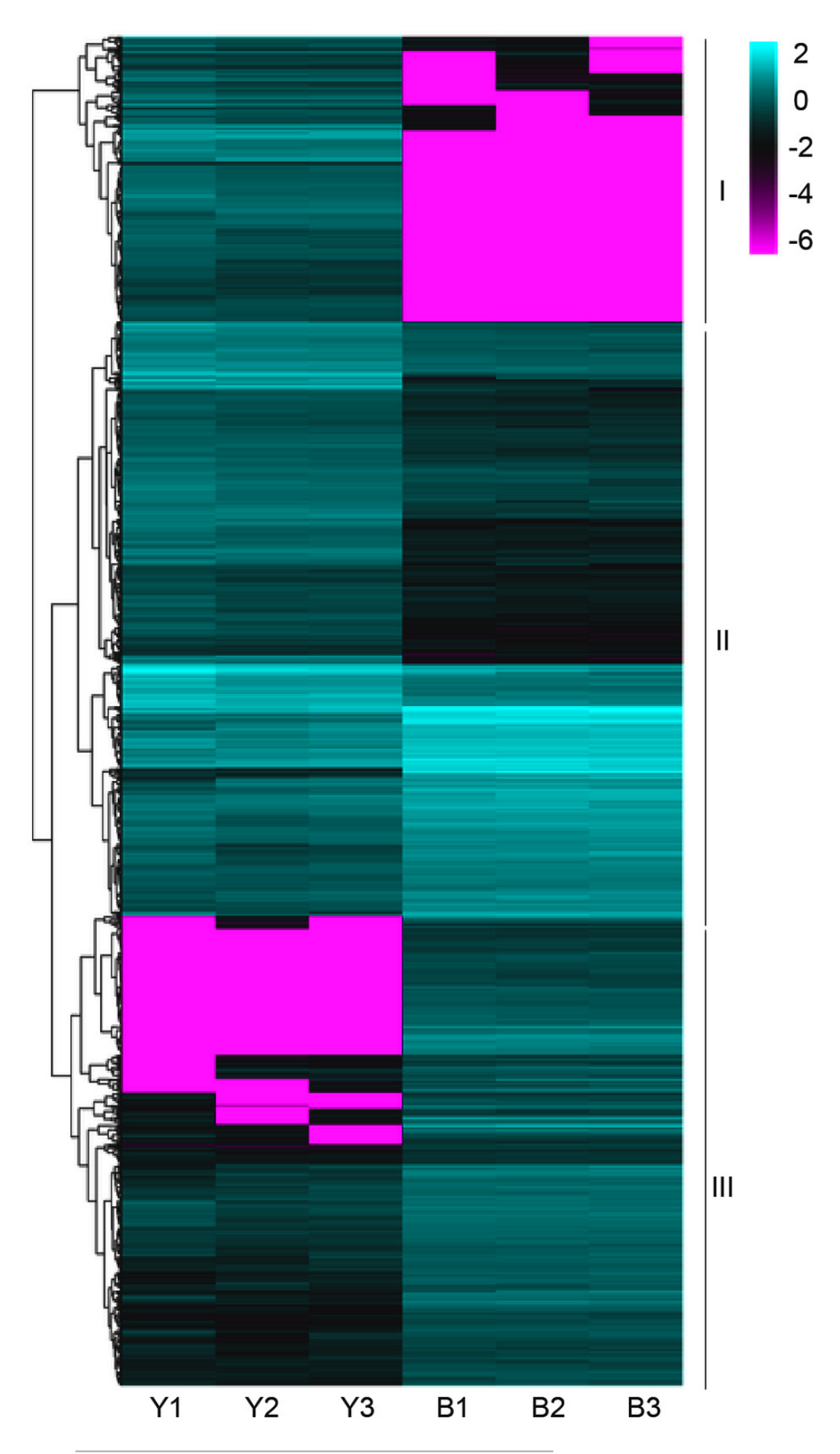




A heatmap of the expression profiles of differentially expressed genes (DEGs).

The expression level was normalized using the FPKM method, and the color scale bar represents this. Y1, Y2 and Y3 correspond to three biological replications of YG1. B1, B2 and B3 are the three biological replications of B100. DEGs with the same or similar expression pattern were clustered.



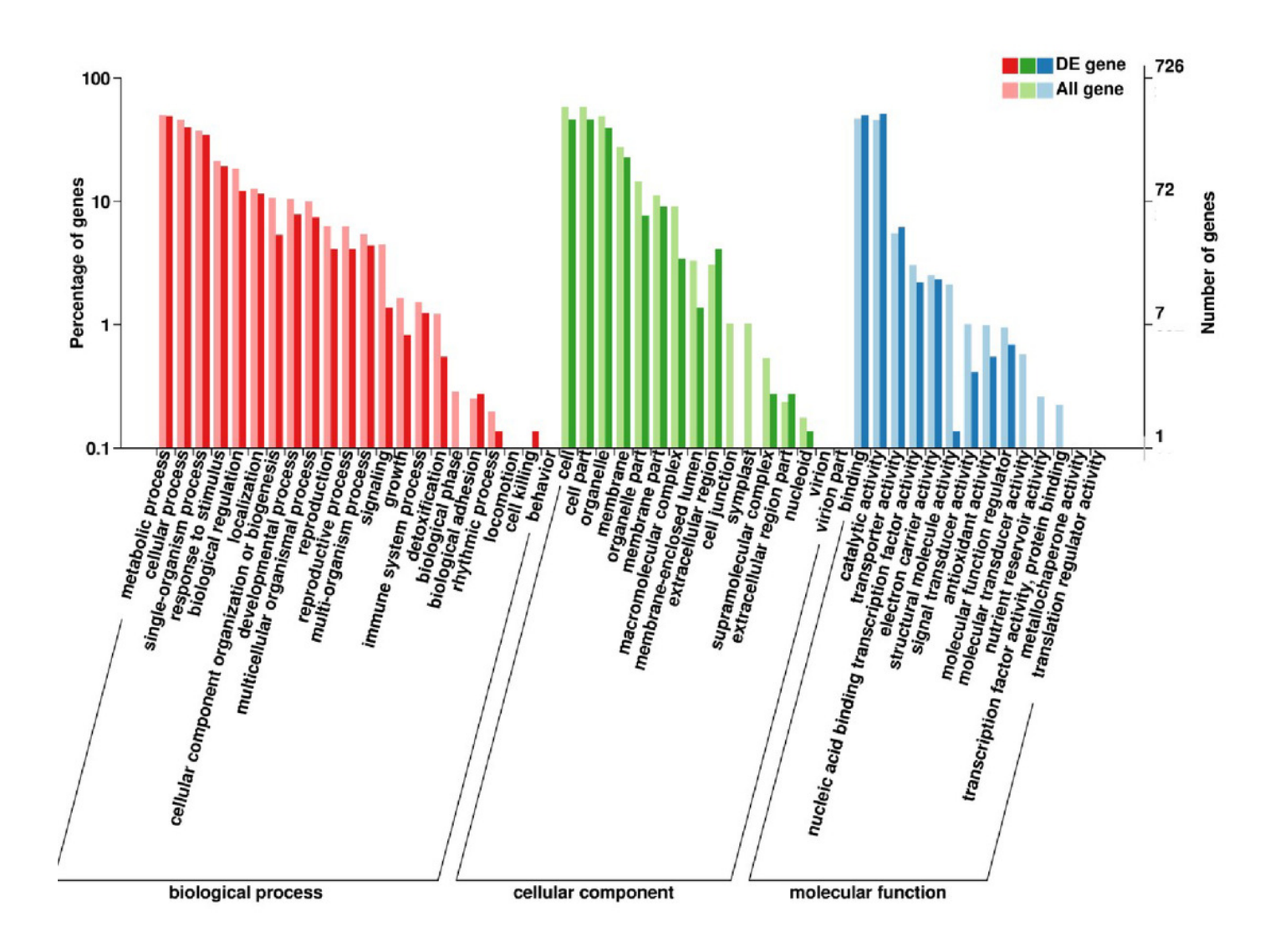


PeerJ reviewing PDF | (2022:02:71153:1:2:NEW 25 May 2022)



GO enrichment analysis of DEGs.

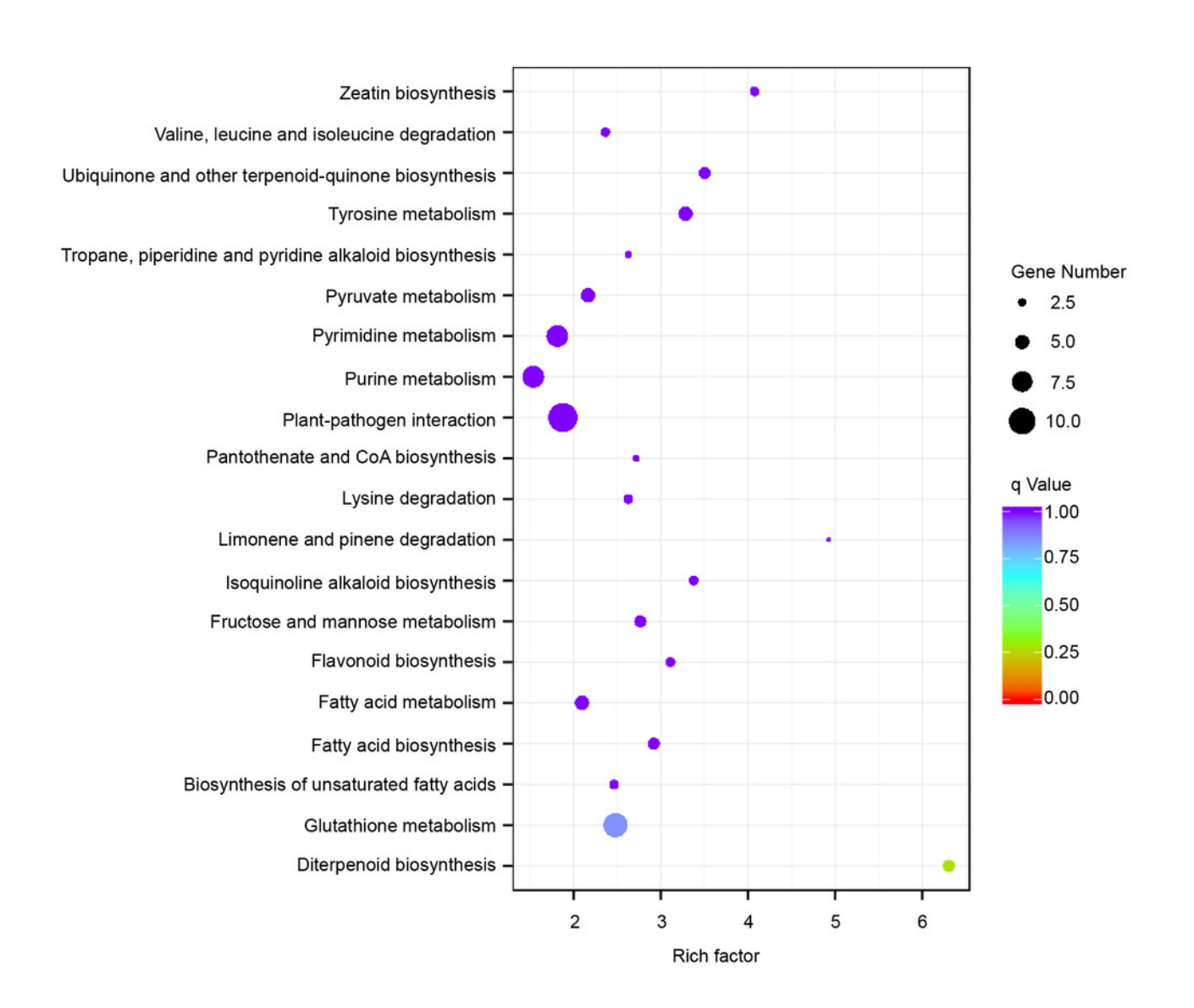
The percentage of DEGs enriched GO terms of the biological process, cellular component, and molecular function are shown.





Enriched KEGG pathways of the differentially expressed genes (DEGs).

KEGG pathways with corrected P-value <0.05 were considered to be significantly enriched. The y-axis shows the description of the corresponding KEGG pathways. The top 20 KEGG pathways enriched in DEGs are shown.





The transcriptional accumulation of enzyme encoding genes of anthocyanin biosynthesis.

The leaves of YG1 and B100 were sampled at 14 days old (seedling stage, SS) and 4 months old (maturing stage, MS). The relative expression levels of these genes were detected by quantitative real time PCR. *ACTIN* (5G464000, Seita) was used as an internal control. Two (**) and three (***) asterisks represent P < 0.01 and P < 0.001, respectively; ns represents no significant difference (n = 3, ANOVA).



